Transactions on Electrical and Electronic Materials (2023) 24:102–114
https://doi.org/10.1007/s42341-022-00423-7

Online ISSN 2092-7592
Print ISSN 1229-7607

REGULAR PAPER

Wear-Induced Attenuation on Transmission Lines and Their Causes

Philipp Lenz[1] · **Philipp Baron**[1] · **Armin Wittmann**[1] · **Georg Fischer**[2]

Received: 29 August 2022 / Revised: 18 October 2022 / Accepted: 27 October 2022 / Published online: 15 November 2022

Abstract
In this paper, the radio frequency (RF) behavior of mechanically stressed coaxial and for the first time also twisted-pair transmission lines is investigated over their service life. The main goal is to enable predictive maintenance for cables in moving applications and avoid preventive replacement. This also reduces the use of high-cost resources. For this purpose, stranded and solid-core variants of coaxial and twisted-pair type cables are mechanically loaded on the two-pulley apparatus according to EN 50396. Their RF transmission (S21) behavior is measured using a vector network analyzer and presented over bending cycles. For the first time, the phase response of mechanically loaded transmission lines is evaluated with respect to their service life. Two significant causes for the increasing attenuation and altered phase response are identified: breakage in foil screen and increasing surface roughness on the copper conductors. The identified causes are supported with literature evidence. Through measurements and theoretical calculations, it is proven that the phase is much more suitable for an assessment of the remaining service life than the amplitude. The findings can be used to implement a cable monitoring system in industrial environments which monitors the lines in-situ and reminds the user to replace them, whenever a certain wear-level is reached.

Keywords RF attenuation · Coaxial · Twisted-pair · Transmission phase · Surface roughness · Wear-level monitoring

1 Introduction

Cables in moving applications have a limited service-life. Thus, failure is merely a matter of time. Such breakdowns imply downtime of the application and usually mean loss of productivity or other economic damage. As a countermeasure, cables are replaced on a regular basis before their end-of-life (EOL) is reached. This creates downtime and cost that can be averted if a monitoring system is in place. A further environmental benefit is the reduced need for copper. As with many mineral resources, it is known that the extraction of copper has caused dire ecological consequences [1] and continues to do so [2, 3]. In summary, economic and ecological potentials can be raised if the replacement of lines, which are still in working order, is prevented. Demand for copper is at an all-time high and will continue to rise in perspective [4, 5]. Therefore, and due to the increasing environmental impact of copper [5], preventive replacement is ecologically and economically not advisable. In the future, a predictive maintenance approach will be used to make optimum use of the service life of a cable in its application. For the successful application of this approach, a measured value that provides information about the current/actual wear condition of the cable is a mandatory prerequisite.

The transmission properties of conductors can be measured in-situ with appropriate methods and can thus be used to evaluate the condition of the conductor during operation. In addition, a combination of an embedded conductor and evaluation electronics can serve as a sensor system to evaluate the condition of the surrounding material such as natural fiber composites [6].

As a solution, the evaluation of the transmission properties at high frequencies is presented here. For connectors, it is known that the RF parasitic phase modulation originating from mechanical movement increases over the connectors mating cycles [7]. However, this damage is limited to a small section of the transmission line compared to the utilized wavelength and is thus only partly comparable to a cable which is loaded

✉ Philipp Lenz
Ph.Lenz@etech.hochschule-trier.de

[1] Laboratory for Applied Production Engineering, Trier University of Applied Sciences, 54293 Trier, Germany

[2] Institute for Electronics Engineering, Friedrich-Alexander-Universität Erlangen-Nuremberg, 91058 Erlangen, Germany

over a wide area. While [8] states, that parasitic amplitude and phase modulation occur for cables under motion, the long-term behavior over the conductors service-life was not regarded yet. The idea for monitoring the RF amplitude of a mechanically stressed cable over its service life was first proposed by Ehlenz [9] as part of his doctoral thesis. An initial verification of the approach using RG58 cable indicated measurable changes in transmission under bending load [10]. While [9] only suggests roughness as a cause, in this paper more comprehensive investigations of the lines are conducted to provide a holistic view of the mechanical wear behavior and thus the causes of attenuation. Consequently, two main reasons for increase of transmission attenuation are identified. In addition, the influence of the measurement frequency used will be presented in more detail to investigate a possible "ideal" measurement frequency for future applications.

Measurements are conducted on two selected coaxial conductors and the behavior is confirmed on two types of twisted-pair conductors. The refined measurement setup allows for the failure behavior to be characterized more precisely. In addition to transmission loss, transmission phase is shown for the first time for evaluation in complex wear situations and explained based on theoretical calculations and practical observations. As already shown several times on different examples such as coaxial lines and PCB traces [11–15], especially the roughness of conductor materials has a proven influence on the RF properties. Therefore, the measurement results are particularly contrasted with the measured RMS roughness Sq, which is evaluated as a potential cause, alongside a detailed optical inspection.

2 Methods

2.1 Fundamentals

As [16] shows, it is assumed that the skin effect has a purely resistive effect. Therefore, a sensitivity analysis is conducted to show the theoretical influence of an increasing resistance per unit length R′ on the complex propagation constant ɣ. The equation for a general transmission line is given by:

$$\underline{\gamma} = \sqrt{(R' + j\omega L')(G' + j\omega C')} \tag{1}$$

Equation 2, for the case of a lossless transmission line (R′ = G′ = 0), is reduced to:

$$\underline{\gamma_0} = \sqrt{j\omega L' \cdot j\omega C'} = j\omega\sqrt{L'C'} = j\beta_0 \tag{2}$$

In this case the characteristic impedance Z_0 is given by:

$$Z_0 = \sqrt{\frac{L'}{C'}} \tag{3}$$

For high frequencies and low losses (R′ << ωL′, G′ << ωC′), a common [17, p. 17, 18, p. 170, 19, p. 63] approximation for the real part $\alpha = \alpha_R + \alpha_G$ is:

$$\alpha_R = \frac{R'}{2}\sqrt{\frac{C'}{L'}} \tag{4}$$

$$\alpha_G = \frac{G'}{2}\sqrt{\frac{L'}{C'}} \tag{5}$$

According to [17] the phase constant can be identified for the lossy transmission line case by using the 1st order terms of a Taylor series expansion of the propagation constant and the characteristic impedance:

$$\beta = \beta_0\left(1 + \frac{1}{2}\frac{R'}{\omega L'}\right) = \omega Z_0 C' + \frac{1}{2}\frac{R'}{Z_0} \tag{6}$$

The sensitivity of α and β to variations in R′ (caused by an increasingly rough surface e.g.) can be evaluated by forming the partial derivative with respect to R′:

$$\frac{\delta\alpha}{\delta R'} = \frac{\delta}{\delta R'}(\alpha_R + \alpha_G) = \frac{\delta}{\delta R'}\left(\frac{R'}{2}\sqrt{\frac{C'}{L'}} + \frac{G'}{2}\sqrt{\frac{L'}{C'}}\right) = \frac{1}{2Z_0} \tag{7}$$

$$\frac{\delta\beta}{\delta R'} = \frac{\delta}{\delta R'}\left(\omega Z_0 C' + \frac{1}{2}\frac{R'}{Z_0}\right) = \frac{1}{2Z_0} \tag{8}$$

Thus, attenuation and phase-shift are to be expected in transmission measurements of rough conductors. The mathematical solution suggests that an increase in surface roughness in combination with the skin effect equally affects phase and attenuation constant, but phase alterations are easier to detect than amplitude alterations. This can easily be demonstrated, when the propagation constant of a conductor (decomposed for attenuation constant α and phase constant β) is compared to the uncertainty of the measurement equipment. For the CLF200 specimen (Z_l = 50 Ω, l = 0.6 m, C′ = 80.3 pF/m, L′ = 0.2 µH/m, R′ = 33.7 Ω/km, G′ = 13.5 mS/km) described later, the following values can be calculated (cf. Eqs. (4)–(6)):

$$\alpha = \alpha_R + \alpha_G = 6.74 \cdot 10^{-4}\frac{1}{m} \tag{9}$$

$$\beta = 121\frac{1}{m} \tag{10}$$

$$\underline{S}_{21} = e^{-\underline{\gamma}l} = e^{-\alpha l} \cdot e^{-j\beta l} \tag{11}$$

$$\left|\underline{S}_{21,\mathrm{dB}}\right| = 20 \cdot \log\left(e^{-\alpha l}\right) = -0.0035\,\mathrm{dB} \tag{12}$$

$$arg\left(\underline{S}_{21}\right) = \beta l = 72.6\,\text{rad} = 4,163° \tag{13}$$

The datasheet of the utilized VNA (described later) states a measurement uncertainty (transmission, > 2 MHz, Level Range -40 dB to 0 dB) of 0.14 dB and 1.4°. Thus, even if the sensitivity of alpha and beta towards changes in the resistance per unit length is equal, the impact on beta is more valuable, as phase alterations are easier to detect. This hypothesis will be discussed in the following results.

2.2 Specimens

Impedance-controlled lines of different configurations were used as test subjects: In accordance with [10] coaxial cables with a characteristic impedance of 50 Ω were used. While measurements on rigid conductors usually yield faster results and show less scatter, stranded conductors must also be considered for more generally valid statements. The coaxial test subjects therefore include CLF200 [20] with a solid inner conductor and Hyperflex 5 [21] with a stranded inner conductor. Both subjects have a foil shield and at least one braided shield as return path in a coaxial arrangement.

For twisted-pair cables ($Z_0 = 100$ Ω), the procedure is similar: Cables with S/FTP construction and four pairs of Category 7 conductors are used. "Helukat 600" has solid inner conductors of approximately 0.259 mm^2 consisting of pure copper (S/FTP 4 × 2 × AWG 23/1) [22]. The test specimen with stranded inner conductors "Helukat 600 flex" has a total electrical cross-section of approximately 0.128 mm^2 consisting of seven wires (S/FTP 4 × 2 × AWG 26/7) [23].

2.3 Generation of Defects

The two-pulley apparatus according to EN 50396 [24] was used to induce homogeneous mechanical load to all test subjects. The standard describes non-electrical tests on moving cables and lines. The associated apparatus enables homogeneous loading of the test subjects over at least 60 cm with scalable test speed. Because of the two-pulley setup,

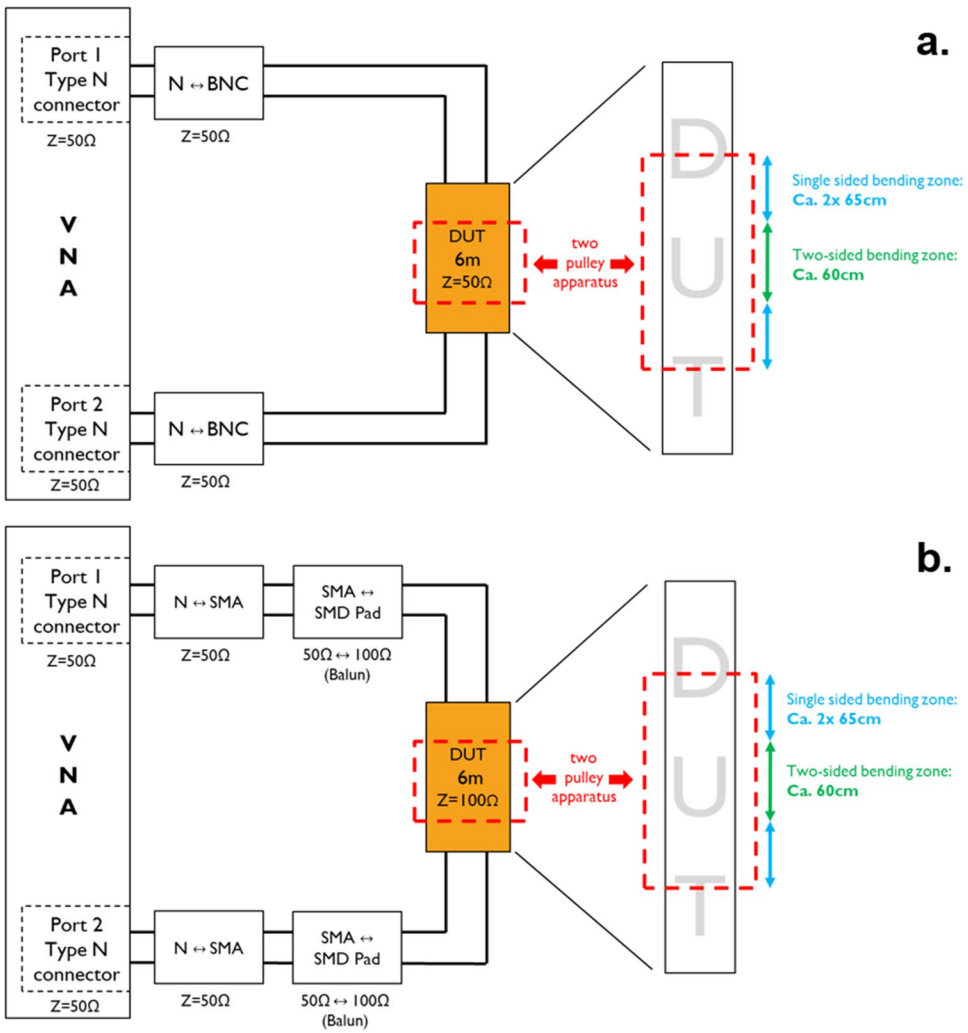

Fig. 1 Block diagram of the measurement setup; a. shows the setup for 50 Ω subjects, b. for 100 Ω subjects

three sections with different loading exist (see Fig. 1). The specimens experience a single-sided bending in the two outer sections resulting in a partially loaded conductor. The inner section is bent in both directions and is thus damaged more. All analysis focus on the inner section as breakage occurs here first. However, it should be noted, that during electrical measurements, the partially damaged areas cannot be excluded and are therefore measured alongside the inner section.

The setup allows a reproducible and scalable assembly of wear patterns, especially by adjusting the roller diameters to suit the respective test subjects. Comparability of the damage behavior is given, since according to the Euler–Bernoulli beam theory there is a correlation between specimen diameter and radius of curvature [25, p. 171]. Specifically, smaller rolls should be used on the bending machine for stranded inner conductors to ensure comparable mechanical bending stress between specimens.

Since specimens on the two-pulley apparatus are subjected to a tensile force by the loading weights, elongation of the specimens is to be expected. Therefore, a length measurement is made by means of a wire-draw encoder at both ends of the specimen. The elongation l is calculated from the sum of the two measured values l_1, l_2 minus start value l_0:

$$l = l_1 + l_2 - l_0 \tag{14}$$

To systematically record causes of the measured attenuation, all test specimens are dissected layer by layer according to their structure from the outside to the inside. This is done in a graded manner according to cycles to document the temporal progression of the damage and is captured pictorially.

2.4 Definition End-of-Life (EOL)

For this paper, the electrical properties are to be plotted against the mechanical wear condition of the conductor. To enable this, it is first necessary to define the EOL condition corresponding to 100% wear or 0% remaining service life. This point is determined by loading the test specimen with the appropriate parameters on the two-pulley apparatus until electrical continuity is interrupted. All conductors of each specimen are connected in series for this purpose. The continuity measurement is carried out with the Bender GM420 loop monitor [26] at 20 mA DC current. Since the resistance of thin data lines alone can already reach a few 10 ohms including connectors etc. and in order to guarantee tripping only in the event of breakage, the trigger threshold is set to 50 Ohm for the loop resistance and a trigger delay of 0 s is set. Monitoring of the DC continuity is adequate because with the smallest interruption in energy or data transmission at the latest, the cable is no longer considered functional in the application and needs to be discarded. The number of completed cycles of the apparatus, in the moment when loop monitoring is triggered, is then set as 100% mark (EOL). Since there is some variance from test to test even within the same batch, the values from multiple measurements are averaged. The number of subjects from which the EOL value is calculated is given in each case along with the standard deviation. Gradations between a new conductor and a defective conductor are created according to percentage of the maximum number of cycles.

2.5 RF Setup

The block diagram of the electrical measurement setup for lines with a characteristic impedance of 50 ohms is shown in Fig. 1a. A PicoVNA 106 from Pico Technology [27] is used as vector network analyzer (VNA). The widest possible frequency band from 10 MHz to 6 GHz was chosen to acquire the values. Within this frequency span, 5001 frequency points are resolved. No averaging is performed, but all values were confirmed mesuring a second sample. The VNA is calibrated in advance using the FSH-Z28 standard from Rohde & Schwarz for open, short and load. A 1.829 m long test lead of type Sucotest 18 [28] serves as through standard. The calibration plane is thus at the level of the connectors of the VNA. For all result plots, a measurement of the respective new subject is used as a reference and all subsequent measurements are shown relative to it.

For the adaptation of the measurement equipment to twisted-pair lines with a characteristic impedance of 100 ohms, an impedance matching element is required. This is formed by a balun (type Macom MABA-011100 [29]) located on a custom PCB (cf. Fig. 2) inside a shielded enclosure near the two-pulley apparatus. An O-type attenuator of 6 dB is also located on the PCB to suppress reflections. The associated block diagram is shown in Fig. 2c. This PCB is also used to ensure proper contacting of a pair of conductors from the twisted-pair composite. This is done by clamping the conductors onto the exposed pads with a PTFE block (see Fig. 2b). Since this connection is not exposed to movement or mechanical forces and remains unchanged until the end of the tests, the evaluation of the repeatability of the electrical connection was omitted.

Both magnitude and phase of the forward wave gain (S21) are evaluated for this paper. To compensate for inadequacies in the setup, all measured values are presented relative to the reference measurement. This is carried out with a new conductor, which is placed in the ready-to-use apparatus at the beginning of the measurement series. Compromising of contact points is excluded by maintaining the contact

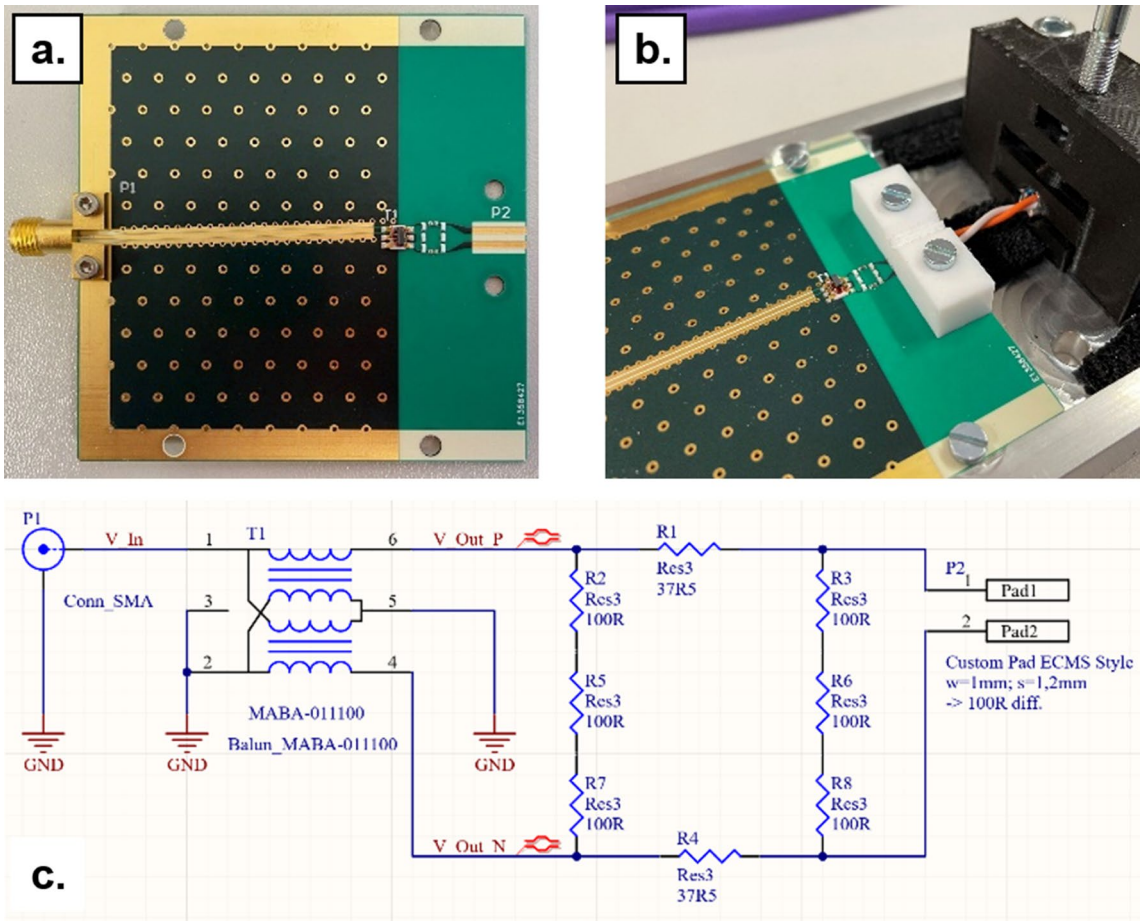

Fig. 2 Impedance matching PCB with attenuation network for measurement of 100 Ω specimens

over all measurements and not moving the setup (except for the moved conductor section). After every n cycles, the movement sequence is briefly stopped for the time of the measurement and then continued.

2.6 Optical Inspection

For the systematic analysis, specimens are disassembled step by step after 100% of the cycles on the two-pulley apparatus. In the corresponding figures, the individual stages of the disassembly are shown for the new conductor and for the loaded conductor side by side.

The development of roughness on the surface of mechanically loaded conductors is known to be a key wear mechanism [6]. In this paper, the measured attenuation is compared to the roughness at the conductor surface. Corresponding measurements are carried out with the aid of the confocal Microscope Confovis Toolinspect S [30]. Evaluation of the 3D data of the surface texture are performed with MountainsMap software from Digital-Surf. The surface is first aligned to remove possible errors caused by tilting of the specimen relative to the image plane. Areas with insufficiently dense datapoints are excluded from the measurement. Subsequently, the shape is removed from the dataset with a fourth-degree polynomial. The roughness parameter Sq is subsequently calculated for the processed surface. Compared to popular line-based roughness Rq, the choice of the area-related value Sq offers the advantage that the choice of the underlying line profile is omitted and thus has no influence on the measured values.

$$\mathrm{Sq} = \sqrt{\frac{1}{\mathrm{A}} \iint_{\mathrm{A}} z^2(x, y)\, dx\, dy} \tag{15}$$

The definition of the area-related RMS roughness is shown in (15).

Macroscopic pictures are acquired using a Leica M205 C stereo microscope [31].

3 Results

3.1 Attenuation of Transmission

Loading of all specimens was carried out on the two-pulley apparatus according to EN 50396 as mentioned in chapter II. Cables with solid (inner) conductor (CLF200, Helukat 600) are treated with a roller diameter of 80 mm and samples with stranded (inner) conductors (Hyperflex 5, Helukat 600 flex) with 35 mm rollers. For all subjects, 1.5 kg of loading weight was applied, acceleration was set to 4 m/s^2, velocity to 0.5 m/s and a current of 20 mA was applied for continuity measurement. Results of the determination of the EOL cycle count are shown in Table 1.

Table 1 EOL mean cycle count for all test subjects, number of samples tested and standard deviation

Subject	No. of samples tested	Mean cycles to EOL	Standard deviation of mean cycles
CLF200	3	731	29 (4%)
Hyperflex 5	4	1126	90 (8%)
Helukat 600	3	1753	121 (6.9%)
Helukat 600 flex	5	803	135 (16.8%)

Results of the attenuation measurements for all specimens are summarized in Fig. 3. Selected measurement frequencies are shown color-coded. As expected, attenuation increases with frequency for all samples with the exception of 2.4 GHz on the CLF200 specimen (Fig. 3a). The deviation is expected to be an outlier caused by interference with wireless LAN service in the test area. The observed increase in attenuation is significant for all subjects compared to ripple in the graphs. A separation of 2.5 dB to 3.5 dB between a new and an EOL conductor is reached for the coax-type subjects and 8 dB to 10 dB can be observed for twisted-pair samples when using a test frequency of 4.8 GHz. As the most distinct results are achieved at highest frequency of 4.8 GHz, further analysis focuses on the data related to this frequency.

The influence of mechanical load on the transmission loss is apparent for all graphs in Fig. 3. Unlike expected, attenuation does not increase monotonically with cycles on the loading machine for all specimens. A clear stagnation of the measured values can be observed for Hyperflex 5 (Fig. 3b) and Helukat 600 (Fig. 3c). Especially the early stagnation for Helukat 600, starting at approx. 400 cycles of loading, may represent a challenge that cannot be neglected

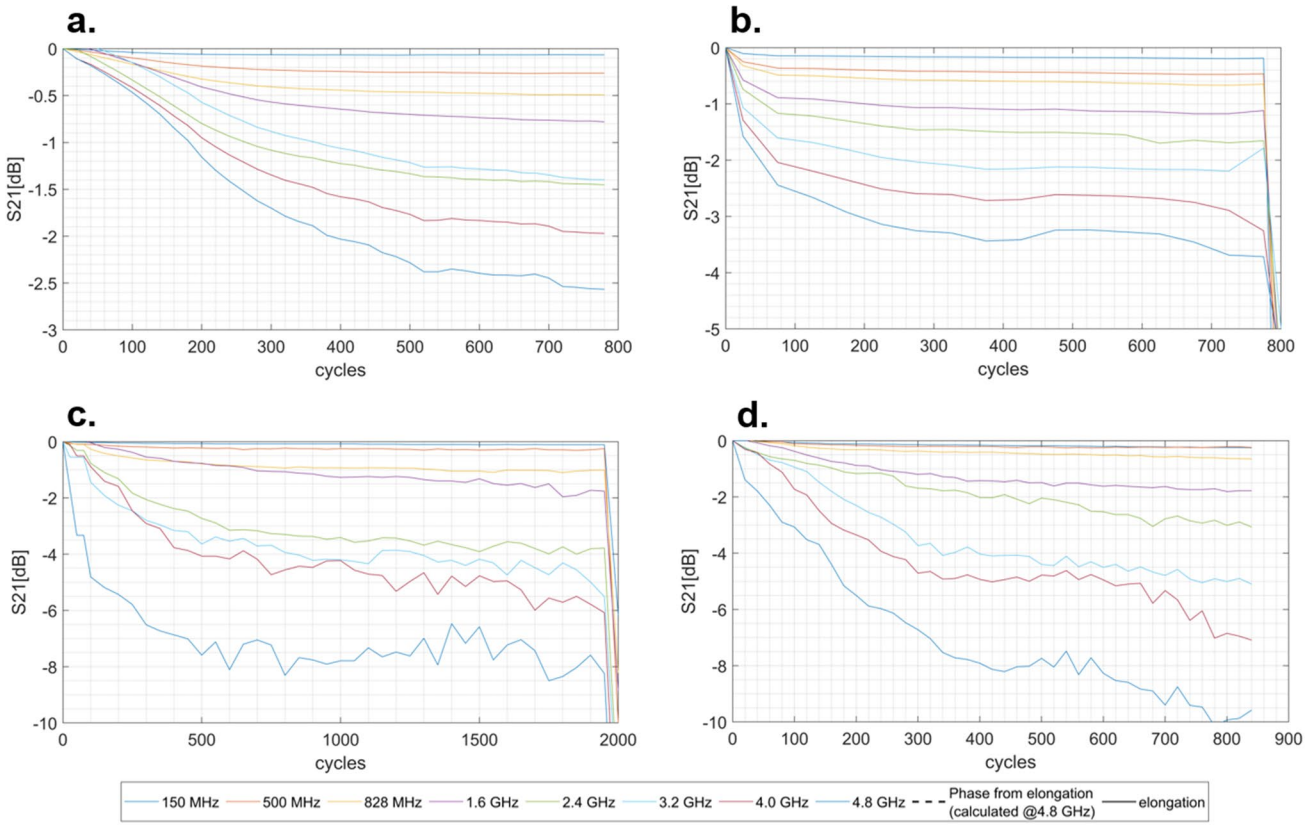

Fig. 3 Magnitude of Forward wave Gain (S21) of CLF200 (**a**), Hyperflex 5 (**b**), Helukat 600 (**c**) and Helukat 600 flex (d) plotted against cycles on two-pulley apparatus for different frequencies (color-coded)

for future applications as it prevents the use of this value to evaluate the wear-level in-situ. Notably, the stagnation is present for all presented frequencies.

Sudden and steep increases in attenuation at high cycle counts for Hyperflex 5 (Fig. 3b) and Helukat 600 (Fig. 3c) are explained by breakdown of the respective conductors (continuity interrupted).

3.2 Transmission Phase

A more significant influence of aging on the transmission is shown in Fig. 4. The phase responses of all specimens are plotted alongside the measured elongation. The measured phase is composed of a mechanical and an electrical elongation of the cable. The mechanical elongation was measured with the above- mentioned wire-draw encoder and the data was smoothed with a moving average filter (length of the sliding window: 10 values). From the length, taking into account the velocity ratio, an equivalent phase for a frequency of 4.8 GHz was calculated and also plotted. It can be seen for all subjects, that the measured phase by no means solely arises from the mechanical elongation. According to [17], the roughness has a significant influence on the phase. The derived gradient model shows a clear mathematical influence of the location-dependent conductivity on beta of the propagation constant in the transmission line model. Analogous to the mechanical elongation, this phenomenon can be called electrical (or virtual) elongation.

What is particularly striking is that for all specimen, the steepest slope can be found within the first 100 cycles. This can partly be explained by settling processes where the cables react to the applied tension (from loading weights) with changes in the axial and radial geometry. As geometry of the cable mainly defines its characteristic impedance and propagation constant, slight changes in geometry directly translates to an altered impedance [32, 33], which is a local mismatch and thus leads to losses in transmission. This behavior corresponds to the observed attenuation for Hyperflex 5, Helukat 600 and Helukat 600 flex in Fig. 3.

Figure 4 also reveals the absolute elongation for the different specimens over mechanical load. Cable types that are intended for moving application experience a considerably greater strain than their corresponding counterpart. At first glance, this is contrary to general expectation, since the thicker solid cores have a higher strain reserve. The reason for this behavior is a shift of the strands in the inner conductor due to the bending load

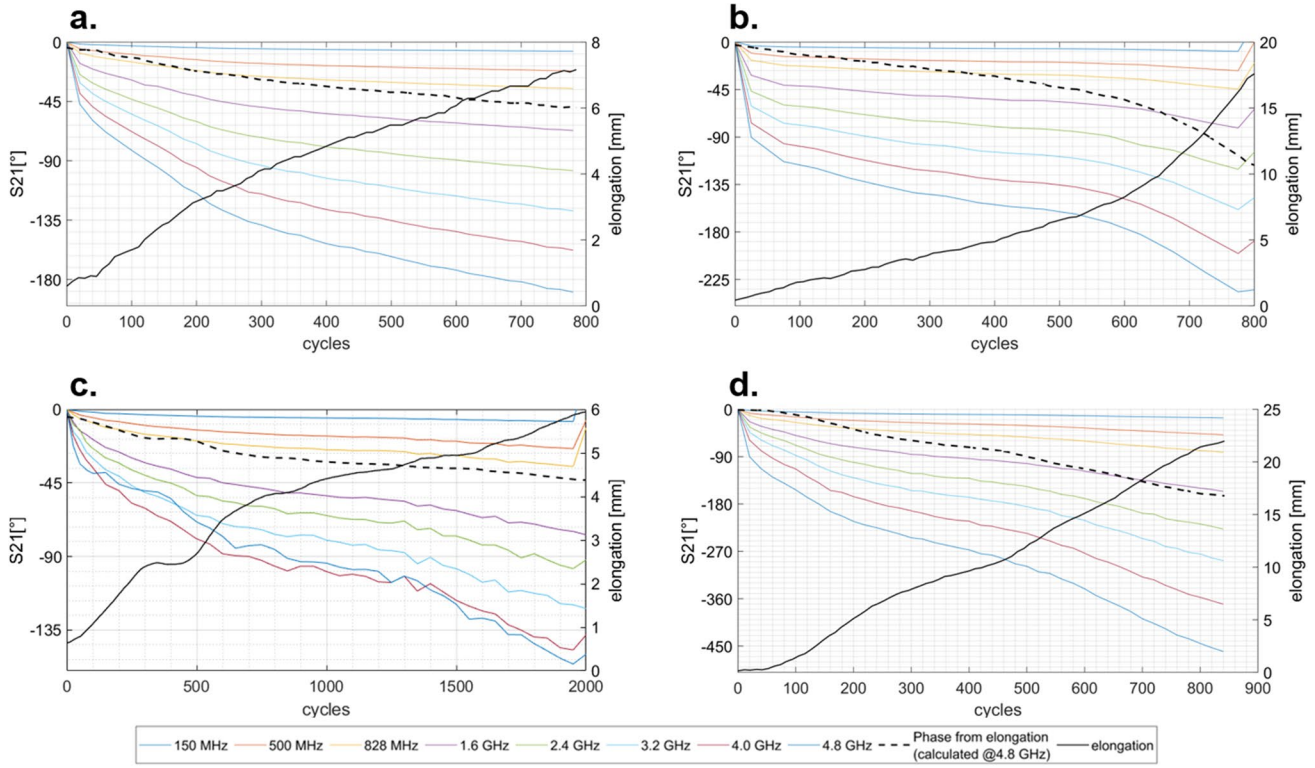

Fig. 4 Phase of Forward wave Gain (S21) of CLF200 (**a**), Hyperflex 5 (**b**), Helukat 600 (**c**) and Helukat 600 (**d**) flex plotted against cycles on two-pulley apparatus for different frequencies (color-coded)

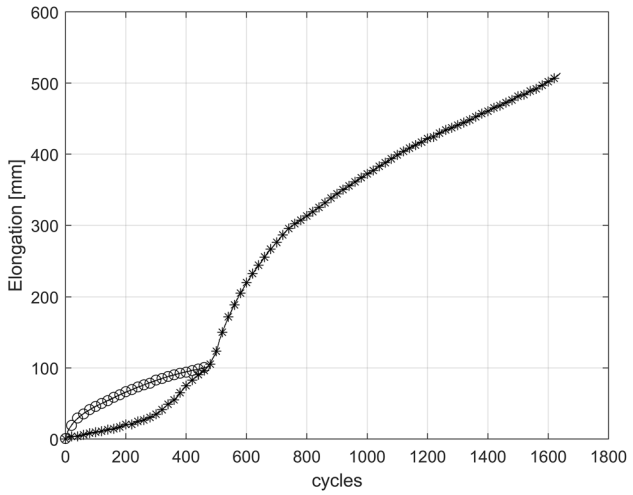

Fig. 5 Elongation of H07V-U (one in 200 datapoints marked with a circle) and H07V-K (one in 200 datapoints marked with an asterisk)

according to EN 50396. The constant tensile load finally ensures that the stranding changes and elongation of the cable becomes possible. This behavior is not possible for test specimens with a solid inner conductor, which is why a significantly lower elongation of the cable is observable. This unintuitive behavior was additionally investigated and confirmed on conductors of type H07V-U and H07V-K (see Fig. 5).

3.3 Optical Analysis of Specimens

To illustrate the causal factors, the coaxial specimens are systematically disassembled as described in the chapter Methods. As twisted pair specimens basically show the same behavior, the presentation of these pictures is omitted.

3.3.1 CLF200

The first electrical layer is the screen, which is composed of braided tinned copper braid and an aluminum foil tape.

Figure 6 shows all relevant layers of the CLF200 subject. Pictures labeled with "a" followed by a number show a new sample, pictures starting with "b" show a sample that has reached EOL. The braid (Fig. 6a1, b1) does not show any mechanical wear such as abrasion or breakage. The relative area covered by the screen (degree of coverage) remains unchanged as well.

The foil screen as depicted in Fig. 6b2, b5 shows signs of abrasion. However, the lack of chips and metallic dust inside the sheath prove that no significant material removal took place. The marks can be regarded similarly to roughness on the surface of a conductor that originates from intrusion and extrusion. However, these marks are facing away from the inner conductor. Considering skin and proximity effect for the geometry of a coaxial cable, the highest current density can be observed on the edges of the conductor that faces its counterpart [34, p. 389]. For the foil screen, most of the current will flow on the side facing the inner conductor. As the skin depth for 2.4 GHz is roughly 1.4 µm, the outfacing roughness on an approx. 30 µm thick foil will not contribute significantly to any attenuation.

Upon inspection of the gas injected polyethylene foam dielectric (Fig. 6a3, b3) no difference between a new and a loaded specimen can be identified.

The inner conductors show a significant increase in surface roughness from the new state (Fig. 6a4) to the EOL state (Fig. 6b4). This roughness is inspected in more detail in chapter Surface Roughness. It represents the only relevant wear mechanism for this type of cable.

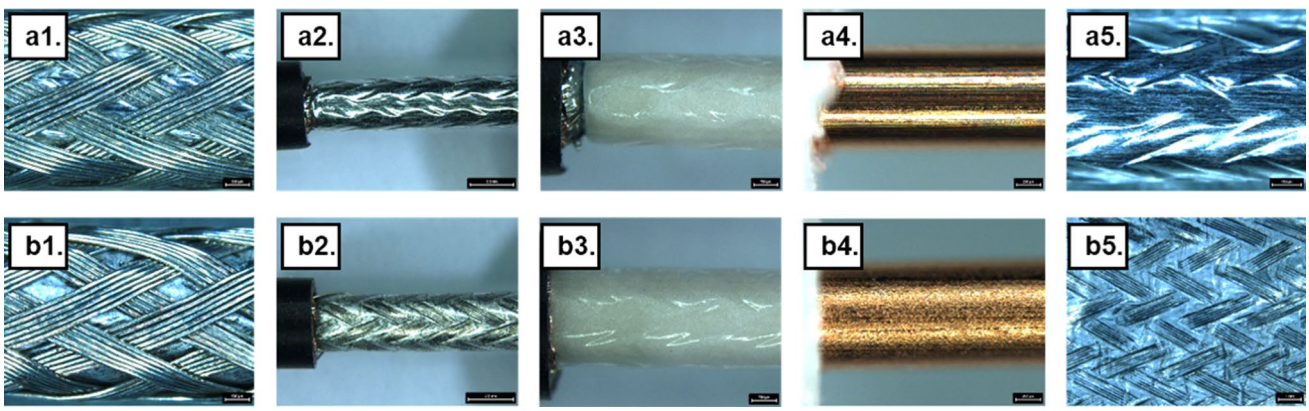

Fig. 6 Sample **a** represents the new conductor, sample **b** the one after 761 cycles on two-pulley apparatus. Figures ×1 show the braided shield, ×2 the foil shield, ×3 the insulation, ×4 the conductor and ×5 unrolled outside of the foil shield

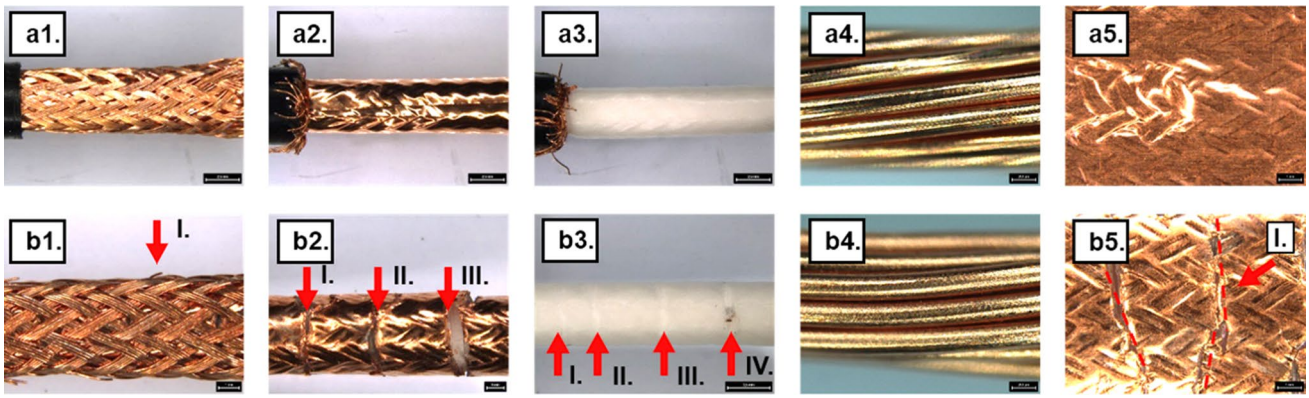

Fig. 7 Hyperflex 5 subject; Sample **a** new, sample **b** in EOL condition

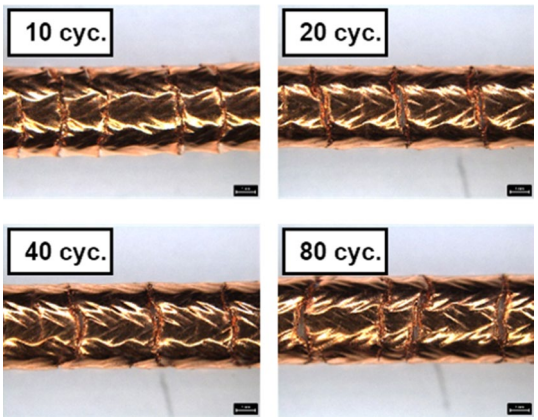

Fig. 8 Breakage of the Hyperflex 5 foil screen can already be observed after 10 cycles on the two-pulley apparatus

3.3.2 Hyperflex 5

The double braid of the loaded Hyperflex 5 specimen only shows minor breaks in the strands of the braid (Fig. 7b1 Mark I). The foil shield is broken several times almost in a ring (Fig. 7b2 Marks I-III). It is only partially held together by its flexible polyethylene coating, which can be seen particularly well in Fig. 7b5 Mark I.

The indentations of the fractures in the foil screen are equally found on the foamed polyethylene dielectric (Fig. 7b3 Marks I-IV). This is a state of inhomogeneous damage, resulting in discontinuities for wave propagation. Due to the compromised geometry, local deviations of the characteristic impedance are likely but small in their influence compared to a ruptured conductor. The large number of fissures in conjunction with the irregular arrangement (cf. Fig. 7b5 dashed line as well as Fig. 7b3 Mark I-IV) and the small spacing ($s < \lambda/10$) make these defects appear as broadband attenuation instead of discrete notches in the amplitude response when plotted over frequency (compare Fig. 10).

With finer grading of the cycles, it can be observed that these fissures already appear in specimens with 10 cycles of loading and only slightly increase in number or widen up afterwards (see Fig. 8). In the outer conductor, the current density becomes maximum towards the dielectric [34], so that with the cracks the maximum layer contributing to the conductivity is interrupted or at least to be considered as a sectionally layered structure. Since grooves transverse to the current direction have a stronger effect on attenuation than those longitudinal to the current direction [35], the same can be assumed for incomplete fissures. Hence, transversal fissures are the dominant influence compared to the small number of breakages in the braid. Moreover, it is known that despite potentially different conductivities of braid and shield, both skin and proximity effect dominate the current distribution in multilayer coaxial setups [36]. The structure with broken shielding resembles a “leaky cable”, where the injected energy is partially radiated at the respective damaged points and thus cannot be transmitted entirely. Therefore, fissures in the foil screen are identified as cause for the strong changes in the frequency response between 0 and 100 cycles in Fig. 3. Figure 7b4 shows a slight increase of surface roughness, which is further investigated in section Surface Roughness.

3.4 Surface Roughness

As shown by [11–15], roughness has a proven influence on the RF performance of transmission lines. Therefore, surface roughness measurements are conducted on all specimens. Performing adequate measurements is challenging for stranded specimens because of (partially severe) deformation (unrounding and burrs) of the strands due to the stranding process in the course of wire production. No valid measurement could be performed on Helukat 600 flex due to

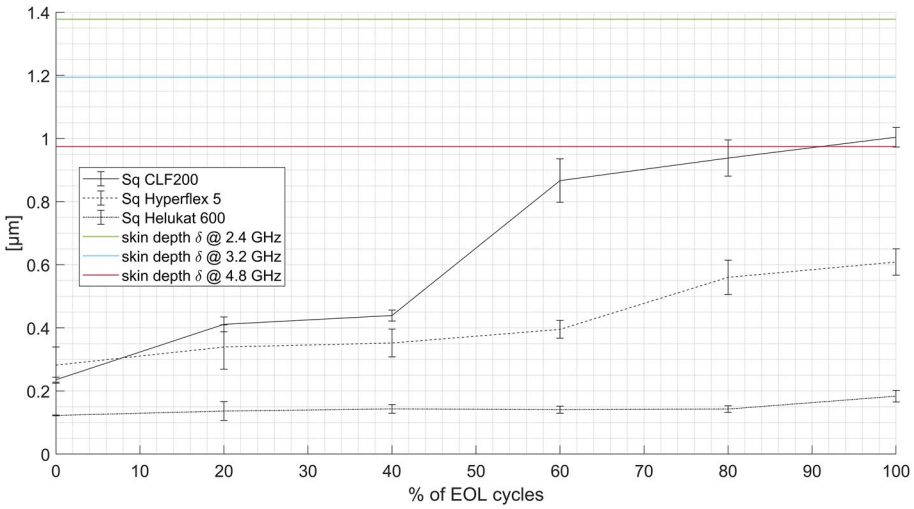

Fig. 9 RMS roughness of CLF200, Hyperflex 5 and Helukat 600 over cycles, each point averaged from min. n = 3 measurements; data acquisition for Helukat 600 flex not feasible; skin depth for reference

its severe deformations in combination with the small strand diameter of approx. 150 µm. In order to perform comparable measurements, the shape of all samples of Hyperflex 5 type (diameter of approx. 300 µm) was removed by a polynomial of the 8th degree, in deviation from the method described. Comparisons between the measurement results of different samples are therefore only possible to a limited extent. However, the values within the sample are suitable to show the course of the development of roughness.

Examinations with the confocal microscope show a clear increase in roughness over the number of loading cycles (cf. Fig. 9) for all specimens. In particular, a monotonous but non-linear progression of the roughness can be observed, as has already been demonstrated with conductors of the H07V-U type [37]. Explanations for the origin of the roughness as well as the non-linear behavior are also given in [37] and will therefore not be further elaborated here.

For CLF200 (diameter 1.1 mm) absolute values for RMS roughness increase from Sq = 0.24 µm in new state to Sq = 1 µm at EOL, which corresponds to a factor greater than 4. Measured strands from the Hyperflex 5 subject increase in roughness from Sq = 0.28 µm to Sq = 0.61 µm. That increase still corresponds to a factor of 2. The roughness on solid cores of Helukat 600 specimens increase from 0.12 to 0.18 µm, which is equal to a factor of 1.5.

It seems reasonable to assume that the resulting absolute roughness after mechanical load is proportional to the diameter of the conductor. This makes sense since larger conductors experience higher stresses in their edge region and more material is available for in-/extrusion. However, this link is beyond the scope of this paper and requires further experimentation and consultation of the relevant literature.

In qualitative terms, approximately doubling of the roughness parameter Sq can be observed. In comparison with the attenuation curve, it must be concluded that the ring-shaped cracks are the dominant influence at low cycle numbers and that the continuous increase in roughness over the course of loading is therefore not sufficient to explain the significant increase of attenuation.

4 Conclusion and Discussion

The transmission behavior of mechanically loaded cables was investigated. Transmission properties are intended to evaluate the remaining service life of cables in moving applications measurable in-situ. In addition, this measurement principle enables the use of cables as a sensor [6]. Due to the high frequencies required, the investigations were carried out on impedance-controlled lines. For the first time, not only coaxial but also twisted-pair types were investigated for their transmission characteristics over service-life. Both, lines with stranded (Hyperflex 5, Helukat 600 flex) and types with solid inner conductors (CLF200, Helukat 600), were used as test subjects. A detailed analysis of the coaxial cables concluded, that two different mechanisms are responsible for attenuated transmission: Roughness and fissures in the foil screen.

The effects of a change in resistance per unit length (for example, due to a resistive nature of roughness) were carried out by a brief analysis of sensitivity in chapter 2.1 Fundamentals. The result states that magnitude and phase should be equally sensitive to changes in resistive per unit length while phase changes are easier to detect. An effect of the mechanical load on the magnitude of the transmission was clearly shown in the measurements, but the specimens (with the exception of the Helukat 600 flex) do not show sufficient slope in the range of interest for a preventive swap around 80% EOL for example. Thus, a robust evaluation of the magnitude alone would be challenging for an industrially deployed system.

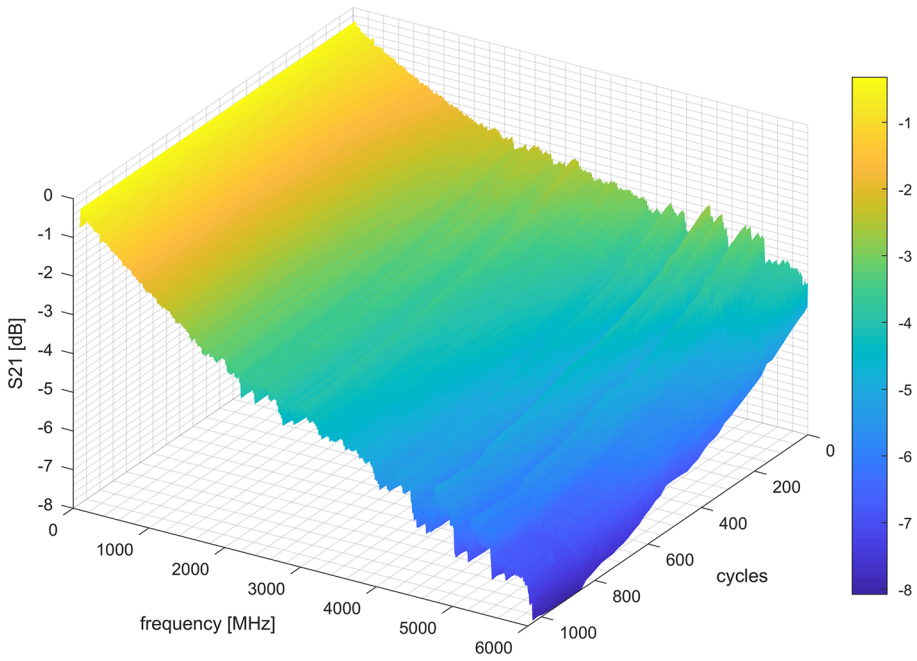

Fig. 10 3-D surface plot for CLF200; Attenuation plotted against frequency and cycles

Following the argumentation of [15], the transmission phase was considered for the first time. Although it is superimposed by the elongation of the test subjects due to tensile load, the graphs clearly show that this elongation cannot be the sole cause. Thanks to the higher slope towards the EOL it can be concluded, that the phase is more suitable than the magnitude for determining the remaining service life of cables in moving applications.

A detailed optical inspection revealed another wear mechanism that is especially relevant for high-frequency measurements. The screen of Hyperflex 5, which is relevant for guidance of RF waves, showed distinctive fissures after only a few cycles. These manifest in strong changes of magnitude and phase of the transmission. The observations are in agreement with the theoretical consideration of the sensitivity and were confirmed (principle of a "leaky cable") by external measurements of the shielding attenuation according to IEC 62153–4-4 (triaxial method). Comparisons between a new and an EOL specimen showed an average difference of 44 dB in screening attenuation throughout the range of 100 kHz to 3 GHz.

The gradient model developed in [17] suggests, that especially an increased surface roughness leads to an altered phase response. While the findings were based on investigations of the underside of PCB traces towards the substrate, comparable current displacement effects can occur in coaxial and twisted-pair conductors. An examination of the formation of roughness on the specimens showed that this is only really pronounced for CLF200 and can be regarded here as causal for the attenuation. The Hyperflex 5 still shows a measurable increase in roughness, but the effect of the broken screen predominates. The same applies to the two twisted-pair test subjects. Presumably, the magnitude of the resulting roughness is related to the diameter of the specimen. This interesting relationship should be investigated further.

The measurement of the transmission, especially the phase, proves to be suitable to measure the wear-level of transmission lines in-situ. There is a wide range of potential applications. In addition to obvious applications such as energy chains or robot arms, supposedly immobile cables and lines (overhead line, underwater cable …) are also possible. If the cable itself is used as a sensor and embedded in another material to monitor its condition, numerous other fields of application arise.

Another conclusion of the investigations is that the various influences can be described qualitatively well, but quantified poorly. This is due to the sophisticated architecture of the cables investigated. A better separation of the influencing factors should therefore be achieved in future by using a test socket. In it, individual wires can be brought into an impedance-controlled configuration. The influences can be separated and quantified by selectively changing individual variables such as roughness without influencing other variables such as geometry.

The series of measurements showed that the effects become stronger with increasing frequency. Therefore, the focus in the evaluation was set on 4.8 GHz. However, the

frequency cannot be increased indefinitely. With increasing frequency, problems with waveguiding grow as e.g. local reflection dominate the results and higher order modes aside TEM may arise. Higher frequencies might be helpful for gaining a high spatial resolution for troubleshooting (see TDR), but for imperfect transmission lines such as standard twisted pair Ethernet cables, these frequencies are hardly controllable. In the present case, results had to be discarded for the twisted-pair candidates at frequencies above 5 GHz. Ideas of matching roughness and skin depth to find an ideal measurement frequency could not be pursued. As Fig. 10 shows, local maxima and minima exist, but don't correlate to the development of roughness or the cycle count despite a frequency resolution of 1.198 MHz in a measurement range from 10 MHz to 6 GHz.

Acknowledgements The authors would like to express their sincere thanks to Klaus Faber AG for their support and Lapp Testcenter Stuttgart for performing shielding attenuation measurements. Confovis Toolinspect S was funded by the Deutsche Forschungsgemeinschaft (DFG, German Research Foundation)—460284478. The project "Intelligent Composite Materials" is funded by the Carl-Zeiss Foundation.

Funding Open Access funding enabled and organized by Projekt DEAL.

Declarations

Conflict of interest The authors have no competing interests to declare that are relevant to the content of this article.

References

1. J.C. Castilla, Environmental impact in sandy beaches of copper mine tailings at Chañaral, Chile. Mar. Pollut. Bull. **14**(12), 459–464 (1983). https://doi.org/10.1016/0025-326X(83)90046-2
2. J. Chen et al., Environmental benefits of secondary copper from primary copper based on life cycle assessment in China. Resour. Conserv. Recycl. **146**, 35–44 (2019). https://doi.org/10.1016/j.resconrec.2019.03.020
3. I. Yolcubal, A.D. Demiray, E. Çiftçi, E. Sanğu, Environmental impact of mining activities on surface water and sediment qualities around Murgul copper mine, Northeastern Turkey. Environ. Earth Sci. (2016). https://doi.org/10.1007/s12665-016-6224-y
4. B.W. Schipper, H.-C. Lin, M.A. Meloni, K. Wansleeben, R. Heijungs, E. van der Voet, Estimating global copper demand until 2100 with regression and stock dynamics. Resour. Conserv. Recycl. **132**, 28–36 (2018). https://doi.org/10.1016/j.resconrec.2018.01.004
5. K.J. Kuipers, L.F. van Oers, M. Verboon, E. van der Voet, Assessing environmental implications associated with global copper demand and supply scenarios from 2010 to 2050. Glob. Environ. Chang. **49**, 106–115 (2018). https://doi.org/10.1016/j.gloenvcha.2018.02.008
6. P. Baron, P. Lenz, A. Wittmann, G. Fischer, Integrity-sensing based on surface roughness of copper conductors for future use in natural fiber composites. IEEE Sens. Lett. (2021). https://doi.org/10.1109/LSENS.2021.3061143
7. R. Enquebecq, et al., Effect of fretting wear damage in RF connectors subjected to vibration: DC contact resistance and phase-noise response, in *2015 IEEE 61st Holm Conference on Electrical Contacts (Holm)*, San Diego, CA, USA, pp. 22–28 (2015)
8. R. Moch, T.M. Gemmer, D. Heberling, Amplitude and phase uncertainty analysis due to cable flexing in robot-based measurement systems, in *2020 Antenna Measurement Techniques Association Symposium (AMTA)*
9. T. Ehlenz, Multiphysikalische Betrachtung von Kabeln und Leitungen unter mechanisch-dynamischer Belastung, Dissertation, LAP, Hochschule Trier, Trier (2019)
10. P. Lenz, A. Wittmann, G. Fischer, Wear-level-monitoring on electrical conductors with high-frequency alternating currents. Frequenz **75**(3–4), 143–146 (2021). https://doi.org/10.1515/freq-2020-0136
11. J. Hoffmann, P. Leuchtmann, J. Ruefenacht, C. Hafner, Propagation constant of a coaxial transmission line with rough surfaces. IEEE Trans. Microwave Theory Techn. **57**(12), 2914–2922 (2009). https://doi.org/10.1109/TMTT.2009.2034214
12. G. Gold, K. Helmreich, *2012 7th European Microwave Integrated Circuit Conference (EuMIC 2012): Amsterdam, Netherlands, 29–30 October 2012 ; [part of the 15th European Microwave Week (EuMW 2012)* (IEEE, Piscataway, 2012)
13. A. F. Horn, J. W. Reynolds, J. C. Rautio, Conductor profile effects on the propagation constant of microstrip transmission lines, in *2010 IEEE MTT-S International Microwave Symposium*, Anaheim, CA, USA, pp. 868–871 (2010)
14. M. Koledintseva, A. Koul, F. Zhou, J. Drewniak, S. Hinaga, Surface impedance approach to calculate loss in rough conductor coated with dielectric layer, in *2010 IEEE International Symposium on Electromagnetic Compatibility*, Fort Lauderdale, FL, pp 790–795 (2010)
15. G. Gold, K. Helmreich, A Physical Surface Roughness Model and Its Applications. IEEE Trans. Microwave Theory Techn. **65**(10), 3720–3732 (2017). https://doi.org/10.1109/TMTT.2017.2695192
16. H. Katzier, *Elektrische Kabel und Leitungen: Technologien, Anwendungen und Anforderungen* (Leuze Verlag, Bad Saulgau, 2015)
17. G. Gold, *Modellierung rauher Oberflächen und Materialcharakterisierung für den Entwurf von Leiterplatten für Hochfrequenzanwendungen* (Verlag Dr. Hut, München, 2016)
18. O. Georg, *Elektromagnetische Wellen: Grundlagen und durchgerechnete Beispiele* (Springer, Berlin, 1997)
19. P.C. Magnusson, G.C. Alexander, V.K. Tripathi, A. Weisshaar, *Transmission Lines and Wave Propagation*, 4th edn. (CRC Press, Cambridge, 2000)
20. Elcard Wireless Systems, *CLF200 Antenna Cable*. Available: http://www.elcard.fi/files/CLF200-DS01.pdf
21. Messi & Paoloni Srl, *Hyperflex 5 /.212"*. Available: https://messi.it/dati/layout/files/cartellaelementi/Hyperflex%205%20-%20Full%20Datasheet%20ENG.pdf

22. HELU KABEL GmbH, *HELUKAT 600: S/FTP 4x2xAWG 23/1 FRNC*. [Online]. Available: https://www.helukabel.com/opc/workarea/suppliers/DNT/documents/pdf/db/1DB_80810_en.pdf
23. HELU KABEL GmbH, *HELUKAT 600 flex: S/FTP 4x2xAWG 26/7 FRNC*. Available: https://assets-cdn.helukabel.com/suppliers/Helukabel/documents/db/HELUKABEL_M80294_EN_GB.pdf
24. *DIN EN 50396 VDE 0473-396:2006-07: Nicht-elektrische Prüfverfahren für Niederspannungskabel und –leitungen* (2006)
25. Z. Huda, *Mechanical Behavior of Materials* (Springer International Publishing, Cham, 2022)
26. Bender GmbH & Co. KG, *LINETRAXX GM420*. [Online]. Available: https://www.bender.de/fileadmin/content/Products/d/e/GM420_D00112_D_XXEN.pdf
27. Pico Technology Ltd, *PicoVNA 100 Series*. Available: https://www.picotech.com/download/datasheets/picovna-vector-network-analyzer-data-sheet.pdf
28. HUBER+SUHNER AG, *SUCOTEST 18: ST18/SMAm/SMAm/72 inch cable assembly*. [Online]. Available: https://www.hubersuhner.com/en/documents-repository/technologies/pdf/rf-stock-assemblies/st18-smam-smam-72inch
29. MACOM Technology Solutions Inc., *MABA-011100: 1:2 Transformer Balun*. Available: https://cdn.macom.com/datasheets/MABA-011100.pdf
30. confovis GmbH, *TOOLinspect*. Available: https://www.confovis.com/optische-messsysteme/toolinspect/
31. Leica Microsystems GmbH, *Stereo Microscopes: TECHNICAL INFORMATION*. Available: https://downloads.leica-microsystems.com/Leica%20M125%20C/Brochures/Leica_M125C_M165C_M205C_M205A_TechData_EN.pdf
32. P. Leuchtmann, J. Rufenacht, On the calculation of the electrical properties of precision coaxial lines. IEEE Trans. Instrum. Meas. **53**(2), 392–397 (2004). https://doi.org/10.1109/TIM.2003.822719
33. X. Dong, M. Lu, X. Chen, Computation of the characteristic impedance of eccentric coaxial transmission lines by boundary element method, in *2008 World Automation Congress*.
34. Z.B. Popović, B.D. Popović, *Introductory electromagnetics* (Prentice Hall, Upper Saddle River, 2000)
35. R. Wang, W. Cui, A rapid estimation of the conductor loss in the rectangular waveguide with rough surface, in *2011 4th IEEE International Symposium on Microwave, Antenna, Propagation and EMC Technologies for Wireless Communications*, Beijing, China, pp. 498–500 (2011)
36. S. Zinal, Steady-state skin effect in multilayer-conductor coaxial lines, in *2014 44th European Microwave Conference*, Rome, pp. 402–405 (2014)
37. P. Baron, P. Lenz, M. Schomer, K.P. Koch, A. Wittmann, G. Fischer, Surface roughness and its structural orientation caused by internal microstructural changes in mechanically stressed copper conductors. J. Mater. Sci. (2022). https://doi.org/10.1007/s10853-022-07579-w